IET Image Processing

Research Article

IET Journals
The Institution of Engineering and Technology

Adaptive Gaussian notch filter for removing periodic noise from digital images

ISSN 1751-9659
Received on 29th June 2018
Revised 21st December 2019
Accepted on 3rd February 2020
E-First on 14th May 2020
doi: 10.1049/iet-ipr.2018.5707
www.ietdl.org

Justin Varghese[1] ✉, *Saudia Subhash*[2], *Kamalraj Subramaniam*[3], *Kuttaiyur Palaniswamy Sridhar*[3]

[1]*Karpagam College of Engineering, Coimbatore, India*
[2]*Centre for Information Technology & Engineering, Manonmaniam Sundaranar University, Tirunelveli, India*
[3]*Karpagam Academy of Higher Education, Coimbatore, India*
✉ *E-mail: justin_var@yahoo.com*

Abstract: Periodic noise corrupts digital images during acquisition and transmission stages by adding repetitive patterns. This study introduces a new adaptive Gaussian notch filter (AGNF) in Fourier transform domain for effectively restoring images contaminated with periodic, quasi-periodic and Moiré pattern noises. Since periodic noises are sinusoidal functions added to the uncorrupted images, Fourier transform of images make these noisy functions to concentrate as easily distinguishable conjugate peaks in frequency domain. The proposed AGNF effectively identifies the noisy peak positions and adaptively quantifies the associated noisy areas by analysing the ratio of averages of frequencies from adaptively varying neighbourhoods. These identified noisy peaks are then diffused by Gaussian notch filter of adaptively varying sizes. The proposed filter ensures maximum diffusion of identified noisy peak areas by maintaining the minimum frequency values from the outputs of overlapping notch filters. Visual and quantitative experimental analysis of the proposed algorithm with mean absolute error, peak signal-to-noise ratio, mean structural similarity index measure and computation time reveals that AGNF is better in restoring images contaminated with periodic noises when compared to other methods.

1 Introduction

Noise degradations make random variations in the intensity of uncorrupted image and are caused due to errors in sensors, scanner circuits, digital cameras and storage devices [1]. Image restoration attempts to recover or reconstruct the uncorrupted image from its noisy version [2, 3]. Periodic noises are signal independent but spatially dependent noises that corrupt digital images by adding periodically or quasi-periodically distributed repetitive patterns when external interferences occur during image acquisition/transmission. Natural images get corrupted with periodic/quasi-periodic noises when sinusoidal/quasi-sinusoidal noisy functions created by external electrical/mechanical interferences get added with pure image contents during image acquisition/transmission stages. Each sinusoidal/quasi-sinusoidal noisy function added with contents of natural images creates individual periodic patterns in images. Hence, a linear combination of sinusoidal functions with different frequencies creates different periodic patterns with different periodicity in images and the amplitude of these sinusoidal functions controls the strength of these patterns. Periodic noises corrupt digital images by adding periodically or quasi-periodically distributed repetitive patterns to the image when electrical interferences occur during image acquisition [4]. These electrical interferences create line drop out, striping and banding effects in the corrupted image and affect reprographic techniques like half-tone printing [5] and cathode ray techniques [6]. Imaging devices with charge-coupled device based cameras create periodic noises due to temperature and voltage variations along with electrical and electro-mechanical interferences [7]. Imaging devices fitted in non-stabilised imaging holders like helicopters/aircrafts create periodic noises due to vibration of imaging holders [8]. Television receivers experience periodic noise based waveforms in the video outputs when the signal strength is low [9]. Experimental analysis on X-ray imaging devices with complementary metal oxide semiconductor-active pixel sensors and scanning transmission X-ray microscopy techniques have shown that these devices create periodic/Moiré patterns while frequently imaging multiple frames/images [10, 11]. Radiations and magnetic induction between circuits of electrical sources exhibit periodic structures like stripe noise, periodic improper illumination and inter-slice variations in the greyscales of images generated by micro-optical sectioning tomography and magnetic resonance imaging (MRI) techniques [12]. Canvas contamination creates periodic structures in paintings [13]. In MRI physics, k-space refers to the Fourier transform of captured MRI and this *k*-space is possibly being corrupted with spike artefacts that generate periodic patterns of stripes/regular wave like fringes in the MRI sensed data due to loose radio frequency coil connections [14]/electrostatic discharge in the receiver cables/excess duty cycle/uncertain humidity conditions [15]. The automatic removal of these periodic noise based macroscopic density artefacts is an important step in Nissl-stained microscopic atlas of whole mouse brain applications [16]. Strain maps of deformed specimens obtained with Moiré interferometry, speckle interferometry and grid methods are prone to be affected with periodic/quasi-periodic noises because of improper grid alignment/sampling/interpolation errors [17]. Periodic noise corrupts remote sensed images by introducing striping and banding effects during Moderate Resolution Imaging Spectroradiometer (MODIS), Hyperion on-board Earth Observation-1 (EO-1), Landsat Thematic Mapper (TV) and Satellite Pour l'Observation de la Terre (SPOT) based imaging processes [18–20]. Since periodic noise affects most of the imaging processes, it is crucial to have periodic noise removal phase as pre-processing stage in most of the image processing/computer vision applications to provide restored version of the image to the subsequent tasks.

Periodic noise mixes its components with other uncorrupted pixel values and is spread throughout the spatial domain image by making the noisy components difficult to be predicted in spatial domain. Further, any spatial domain based direct noise detection process is complicated since it is difficult to predict the spatial pattern/sinusoidal/quasi-sinusoidal function that corrupts the image by addition. Due to this reason, early kernel based filtering attempts [21] find difficulty in providing better restoration. Since periodic/quasi-periodic noises are linear combinations of sinusoidal/quasi-sinusoidal functions, these noises concentrate in frequency domain as high magnitude spectral coefficients and thereby providing impulsive star/spike shaped noisy peaks. Each

corrupting sinusoidal/quasi-sinusoidal noisy function creates a pair of noisy peaks in the mutually opposite quadrants of the frequency spectrum. These noisy peak regions have the largest spectral value at the centre corresponding to the fundamental frequency of the noisy sinusoidal function. The decreasing noisy areas in star shape of the peak are called the noise bandwidth. The positions of these noisy spikes in frequency spectrum depend on the frequency of the sinusoidal/quasi-sinusoidal function that corrupts the image in spatial domain. Sinusoidal/quasi-sinusoidal functions with low frequencies concentrate near the direct current (DC) coefficient while sinusoidal/quasi-sinusoidal functions with extremely high frequencies concentrate at the borders of the Fourier spectrum by providing star/spike shaped peaks. Since spectral coefficients corresponding to periodic noises form noisy peak areas with spike look in the Fourier transformed image, it is easy for restoration algorithms to distinguish corrupted frequencies from other uncorrupted frequencies. These aspects of frequency domain motivated de-noising algorithms to apply their filtering operation on Fourier transform of the given corrupted image for effectively identifying and diffusing noisy regions before generating the final restored image by applying inverse Fourier transform.

Since frequency domain images are symmetric about opposite quadrants, band reject filters reject specific circular bands of frequencies around the centre of the frequency domain image. However, the band reject approaches could not produce effective results since they reject all frequencies that belong to the circular band irrespective of their purity status. In frequency domain, statistics based algorithms replace noisy areas with suitable statistic values determined from the surrounding frequencies. Although these algorithms are good in maintaining image details, their noise attenuation capability is limited since they do not de-noise neighbouring noisy frequencies. Gaussian notch based filters not only reject the central noisy peak but also suppress the neighbouring noisy frequency areas corresponding to noisy spikes. However, the performance of statistics and notch based algorithms depends largely on the accuracy in determining the noisy peak areas. The frequency domain mean filter (FDMF1) [22], frequency domain median filter (FDMF2) [23], windowed Gaussian notch filter (WGNF) [24], interpolation filter (IF), Brickwall reject filter (BRF) and Gaussian notch reject filter (GNRF) [25] algorithms use static windows of fixed sizes to fix the noisy areas and are non-adaptive in nature while identifying noisy peak positions. Gaussian star filter (GSF) proposed by Ketenci and Gangal [26] uses threshold based region identification technique where all the frequency values less than the given threshold are identified as noisy to quantify the noisy areas. The threshold is identified as a function of central peak frequency although the height of the central peak from its neighbouring noisy peak areas differs for different noise types and amount of corruption. Adaptive optimum notch filter (AONF) [7] identifies the noisy peak positions by applying global threshold identified as the average of maximum of all frequency values outside low-frequency region (LFR) and the average of the noise free smooth arc shaped uncorrupted frequency regions at the corners of the image spectrum. However, if the noisy peaks are with large variations in their heights, the global threshold makes prominent mistakes in effectively identifying all noisy peak positions.

The algorithm proposed by Hudhud and Turner [27] identifies noisy peaks by non-automated procedures. The FDMF1, FDMF2, WGNF, GSF and AONF use automated procedures to find the noisy central peak. However, these algorithms make misclassifications in noise detection when applied on noisy peak areas corresponding to strong periodic noise that fall in the LFRs of the Fourier transformed image. Chakraborty *et al.* filter [28] used frequency domain histogram based thresholding operation for identifying noisy areas, but this method produces misclassifications in noise detection when the noise strength is high. The noisy peak detection procedures employed by Sur *et al.* filter [29], windowed adaptive switching minimum filter (WASMF) [30], Laplacian-based frequency domain filter (LFDF) [31], Chakraborty filter [32], Ketenci filter [33] and Ionita filter [34] use static approximation functions but are not adaptive to the noise and image types. Zhou *et al.* [35] proposed a bilateral linear filter operator by incorporating least-squares regression based noise detection and linear operator based de-noising. Chakraborty *et al.* [36] proposed exponential thresholding based automated notch-reject filter by applying Gabor filter for enhancing corrupted peak positions. However, the thresholding function used for identifying the noisy peaks is prone to make errors when the noisy peak positions fall in the LFR. Frequency-domain-based switching median filter [37] applies traditional region-growing technique to generate the noise map from enhanced frequency spectrum. The identified noisy spectral coefficients are then replaced by the median of uncorrupted frequency spectrum determined by recursive median filter. The filter proposed in [38] by Varghese adaptively moves from the DC coefficient in the centre of the image to the border of the image to detect and correct the corrupted frequencies. However, these algorithms address some goals of periodic noise filtering but could not adequately address other image restoration goals. These goals are computational efficiency, adaptation to various noise and image types, accuracy in identifying noisy peaks and its associated areas, efficacy in rejecting corrupted frequencies and preserving thin/narrow edges in restored outputs.

Addressing the limitations posed by existing algorithms, an adaptive Gaussian notch filter (AGNF) in frequency domain is presented in this paper for de-noising periodic, quasi-periodic and Moiré pattern noises from digital images. The algorithm diffuses adaptively determined noisy peak areas by applying notch reject filter whose size better suits the noisy region. The paper has five sections. Section 2 details the proposed AGNF while Section 3, Section 4 and Section 5, respectively, make the experimental analysis, discussion and conclusion.

2 Proposed adaptive Gaussian notch filter

Let y be the corrupted observation of natural image x of size $M \times N$ and $y_{i,j}$ denotes the intensity value at (i, j) such that $0 \leq i < M$ and $0 \leq j < N$. Noisy observation image, y corrupted with periodic/quasi-periodic noises is denoted by

$$y_{i,j} = x_{i,j} + \eta_{i,j} \tag{1}$$

where η is the two-dimensional signal independent sinusoidal or quasi-sinusoidal noise function that affects the uncorrupted image, x. Since η is a sinusoidal or quasi-sinusoidal function, the Fourier transform of y makes the noisy frequencies to concentrate in frequency domain image by providing spiky peak look. These noisy frequencies mixed with signal contents in spatial domain are easily distinguishable when Fourier transform is applied on corrupted image, y. Therefore, the fundamental issues of filtering periodic noise in frequency domain are to effectively detect and diffuse these noisy peak areas from frequency domain image.

The AGNF effectively detects and quantifies the area of periodic noise corruption in frequency domain. These noisy frequencies are then diffused by applying Gaussian notch filter whose window size varies adaptively to suit the noisy peak areas. The flowchart of AGNF is presented in Fig. 1. The proposed AGNF scheme determines the Fourier transform of the input noisy image and shifts its origin to the centre of the image for performing filtering operation in frequency domain and P is expressed as

$$F_{u,v} = \frac{1}{M \times N} \sum_{i-0}^{M-1} \sum_{j=0}^{N-1} (-1)^{i+j} y_{i,j} e^{-\sqrt{-1}\,2\pi\left(\frac{u \times i}{M} + \frac{v \times j}{N}\right)} \tag{2}$$

Here $F_{u,v}$ denotes the Fourier transform of y at position (u, v). The Fourier spectrum P of F makes the noisy frequency detection process easy in real domain and is expressed as

$$P_{u,v} = \sqrt{R_{u,v}^2 + I_{u,v}^2} \tag{3}$$

Here $R_{u,v}$ and $I_{u,v}$ denote the real and complex parts of $F_{u,v}$.

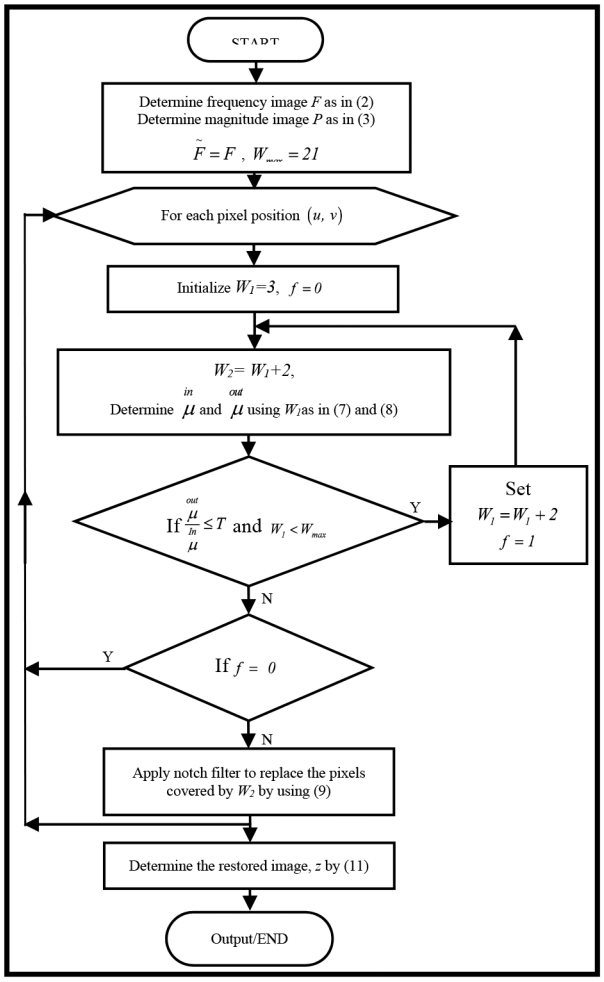

Fig. 1 *Flowchart of AGNF algorithm*

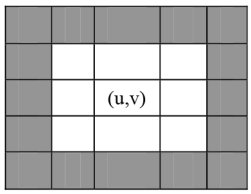

Fig. 2 *Illustration of* $\Omega^{In}_{u,v}$ *and* $\Omega^{Out}_{u,v}$ *when* $W_1 = 3$, □ *denotes* $\Omega^{In}_{u,v}$ *and* ■ *denotes* $\Omega^{Out}_{u,v}$

2.1 Adaptive noisy area identification

The proposed AGNF algorithm adaptively determines the peak areas associated with noisy frequencies of the corrupted frequency domain image by using adaptively varying window approach. The sizes of filtering windows of the proposed filter are adaptively increased from smaller sizes until the windows cover noisy peak areas of Fourier transformed image. The proposed algorithm uses two adaptive windows W_1 and W_2, W_1 being an inner window and W_2 an outer window. For each frequency value, these windows are utilised for finding relative average frequency deviations of frequencies from inner and outer neighbourhoods. If the ratio of the averages of outer and inner neighbourhood frequencies is less than a predefined threshold, the algorithm assumes the frequency positions defined by the inner window as noisy since the frequency values of the inner neighbourhood are extremely higher than outer window frequencies. Let $\Omega^{W}_{u,v}$ represent generalised set of image locations covered by the filtering window with size $W \times W$ at (u, v). $\Omega^{W}_{u,v}$ is defined by

$$\Omega^{W}_{u,v} = \left\{ \begin{array}{l} (j_1, j_2) : u - d \le j_1 \le u + d, \\ v - d \le j_2 \le v + d \end{array} \right\} \quad (4)$$

Here d is the width of the search window, $W \times W$ and is defined by $d = ((W - 1)/2)$. The algorithm first initialises the de-noised frequency domain image $\tilde{F} = F$ assuming that all the frequency positions of F are uncorrupted. The proposed AGNF avoids DC frequency from the filtering process and hence for each frequency spectrum $P_{u,v}$, other than the DC frequency at $((M/2), (N/2))$ and a very small circular portion (a maximum of 6 pixels width) around DC coefficient, the proposed algorithm performs following steps to identify the corrupted frequencies.

Step 1: The algorithm starts by initialising inner window size, $W_1 = 3$, maximum window size, $W_{\text{Max}} = 21$ and the binary flag variable, $f = 0$ indicating an uncorrupted frequency position. The flag variable, f is used for identifying the purity status of frequency $F_{u,v}$.

Step 2: The outer window size W_2 is set to $W_2 = W_1 + 2$. The algorithm uses adaptively varying inner and outer position sets, $\Omega^{\text{In}}_{u,v}$ and $\Omega^{\text{Out}}_{u,v}$ centred at (u, v) for effectively quantifying noisy frequency areas. The frequency values corresponding to $\Omega^{\text{In}}_{u,v}$ and $\Omega^{\text{Out}}_{u,v}$ are used for determining the ratio between the averages of outer and inner frequencies and these neighbourhood sets are, respectively, defined by $\Omega^{\text{In}}_{u,v} = \Omega^{W_1}_{u,v}$ and $\Omega^{\text{Out}}_{u,v} = \Omega^{W_2}_{u,v} \setminus \Omega^{W_1}_{u,v}$ where '\' denotes the set difference operator. The pixel positions covered by $\Omega^{\text{In}}_{u,v}$ and $\Omega^{\text{Out}}_{u,v}$ are illustrated in Fig. 2 for $W_1 = 3$.

Step 3: Since noisy peak areas have very high frequency values when compared to their surrounding frequencies, the algorithm identifies the frequency position $F_{u,v}$ as corrupted when the ratio of averages of pixels from $\Omega^{\text{Out}}_{u,v}$ and $\Omega^{\text{In}}_{u,v}$ is less than a threshold, T. If μ^{In} and μ^{Out}, respectively, denote the average of pixels covered by $\Omega^{\text{In}}_{u,v}$ and $\Omega^{\text{Out}}_{u,v}$ then μ^{In} and μ^{Out} are defined by

$$\mu^{\text{In}} = \frac{\sum_{(i_1, i_2) \in \Omega^{\text{In}}_{u,v}} P_{i_1, i_2}}{\left|\Omega^{\text{In}}_{u,v}\right|} \quad (5)$$

$$\mu^{\text{Out}} = \frac{\sum_{(i_1, i_2) \in \Omega^{\text{Out}}_{u,v}} P_{i_1, i_2}}{\left|\Omega^{\text{Out}}_{u,v}\right|} \quad (6)$$

In (5) and (6), $\|$ denotes the cardinality operation which provides the pixel count in the windows, $\Omega^{\text{In}}_{u,v}$ and $\Omega^{\text{Out}}_{u,v}$. If $\left(\mu^{\text{Out}}/\mu^{\text{In}}\right) \le T$, it is clear that $F_{u,v}$ is a noisy peak position since the frequency values corresponding to the inner neighbourhood, $\Omega^{\text{In}}_{u,v}$ is significantly higher than the frequency values corresponding to the outer neighbourhood defined by $\Omega^{\text{Out}}_{u,v}$. Hence, the flag variable f that denotes the purity status of $F_{u,v}$ is set to 1 indicating $F_{u,v}$ as a corrupted frequency. In this case, when a frequency $F_{u,v}$ is found corrupted, the inner window size W_1 is increased to $W_1 = W_1 + 2$ for quantifying the area of corruption associated with $F_{u,v}$ by continuing from step 2. This process for quantifying the noisy area associated with $F_{u,v}$ is repeated until $\left(\mu^{\text{Out}}/\mu^{\text{In}}\right) > T$ or W_1 has reached the maximum allowed size, $W_{\text{Max}} = 21$. The final outer window size, $W_2 \times W_2$ is determined as the area of corruption and the notch filter of size $W_2 \times W_2$ is used for diffusing the noisy peaks. Although the adaptive window movement of the proposed filter is similar to AONF, the proposed scheme makes better and more accurate region quantification of noisy frequencies than AONF due to its effective ratio based region-growing criteria. The filtering process of the algorithm is explained in the following subsection.

2.2 De-noising process

The noise filtering stage of AGNF diffuses the identified noisy peak areas of $F_{u,v}$ by applying AGNF of size $W_2 \times W_2$. The filter provides identity results when $F_{u,v}$ is uncorrupted. In other words,

```
Procedure AGNF(Noi_Img)
Apply Symmetric padding on Noi_Img
F_In= fft(Noi_Img)
P= sqrt(real(F_In)^2 + imag(F_In)^2)
Th=0.35; L_rgn=6; F_Out=F_In; Wmax=21;
for each pixel (i,j) of P {
  d=sqrt((i-(m/2))^2+(j-(n/2))^2);
  fl=0;
  if (d > L_rgn){
    W1 = 3; cond=1;
    while(cond==1){
      W2 = W1 + 2;
      S1= Average of P covered in W1 × W1
      S2= Average of P covered in W2 × W2
        excluding the pixels in W1 × W1
      if (S2/S1)<=t {
        fl=1;
        if W2>=Wmax :cond=0;else W1 = W1 + 2;}
        else  cond=0;}
    if fl==1 {
      H = Gaussian Notch Filter of size W2 × W2
      Apply H filter in F_Out as in (7)}}}
Img_Out=IFFT of F_Out
Rest_Img= Inverse padding on Img_Out
```

Fig. 3 *Pseudo-code of AGNF algorithm*

after the noise detection stage, if $\left(\mu^{\text{Out}}/\mu^{\text{In}}\right) > T$ and $f = 1$, the algorithm performs the de-noising process of noisy peak areas associated with $F_{u,v}$ by applying Gaussian notch filter of size $W_2 \times W_2$ since the adaptively determined $W_2 \times W_2$ covers the corrupted noisy peak areas associated with the peak frequency $F_{u,v}$ at position (u, v). In this case, for all $(i_1, i_2) \in \Omega_{u,v}^{W_2}$, the notch filtering operation is applied to $F_{u,v}$ for generating the restored frequency domain image, $\tilde{F}_{u,v}$. The notch filtering operation is defined by

$$\tilde{F}_{u+i_1,v+i_2} = \text{Minimum}\left(\tilde{F}_{u+i_1,v+i_2},\ F_{u+i_1,v+i_2} \times G_{i_1,i_2}\right) \tag{7}$$

where G is the Gaussian notch function [7, 25] with single valley in the centre and is defined by

$$G_{i_1,i_2} = 1 - A\mathrm{e}^{-B\left(i_1^2 + i_2^2\right)} \tag{8}$$

where A is the magnitude of the filter and its value lies in the interval [0, 1]. B is a positive scaling constant along rows and columns of G [7]. In (7), the minimum operation makes sure that the algorithm performs maximum diffusion of corrupted frequencies when the Gaussian notch filter corresponding to different noisy peaks overlap each other.

Otherwise, if $\left(\mu^{\text{Out}}/\mu^{\text{In}}\right) > T$ and $f = 0$, then it is clear that current frequency $F_{u,v}$ under consideration is uncorrupted and the algorithm processes the next pixel from step 1 of previous subsection.

Once the algorithm has processed all the frequencies of the frequency domain image, inverses of shifting and Fourier transform are determined to reproduce the final de-noised image, Z as

$$Z_{x,\,y} = \sum_{i=0}^{M-1}\sum_{j=0}^{N-1}(-1)^{i+j}\tilde{F}_{i,j}\mathrm{e}^{\sqrt{-1}\,2\pi\left(\frac{i\times x}{M} + \frac{j\times y}{N}\right)} \tag{9}$$

Here $Z_{x,y}$ denotes the final de-noised image at position (x, y).

Since proposed algorithm performs maximum diffusion of noisy peaks even if the notch filters overlap each other, the proposed algorithm is better in diffusing noisy frequencies and thereby providing better restoration of images corrupted by periodic noises. Fig. 3 shows the procedure/pseudo-code for implementing AGNF algorithm. The proposed AGNF algorithm is advantageous in that it adaptively varies its respective window sizes according to the ratio-based region-growing criteria while identifying and attenuating noisy frequencies depending upon the periodic noise intensity and so it provides better ability in de-noising digital images contaminated with periodic noises.

3 Experimental results and analysis

The experimental simulations are conducted by using Matlab 7 software in an i7 desktop computer with 3.4 GHz speed and 8 GB RAM. The effectiveness of AGNF is compared with ideal low-pass filter (ILPF) [4], FDMF1, FDMF2, WGNF, GSF, Chakraborty *et al.*, AONF, IF, BRF, GNRF, Federic *et al.*, WASMF and LFDF algorithms. The experiment analysis is made with 27 sets of naturally and artificially corrupted images with varying feature and spectral complexities from which the 8-bit Parrot (768 × 512), Lena (512 × 512), Boats (512 × 512), Barbara (512 × 512), Bridge (512 × 512), Brain MRI (191 × 237), Street (1024 × 768), Boy (321 × 480), Mariner 4 (500 × 500), Lower body MRI (331 × 324), Hand written (772 × 682), live football match (367 × 291) and Clown (331 × 324) images are used in this paper for demarcating the effective performance of the proposed AGNF algorithm. These images are selected for comparative analysis of different algorithms according to varying complexities in features, edges and texture details. Similar to other algorithms [7, 29–31, 36–38], the sinusoidal functions that create noisy peaks at frequency spectrum of natural image are used for artificially corrupting images to test the performance of algorithms. These noise functions with strength, a are defined below as N_1 and N_2:

$$N_1(i,j) = a*255\begin{pmatrix}\text{Sin}(1.8i) + \text{Sin}(1.8j) + \text{Sin}(+j)\\ +\text{Sin}(2.2i + 2.2j) + \text{Sin}(1.8i - 1.8j)\\ +\text{Sin}(i - j) + \text{Sin}(2.2i - 2.2j)\end{pmatrix} \tag{10}$$

$$N_2(i,j) = a*255\begin{pmatrix}\text{Sin}(1.1i + 1.1j) + \text{Sin}(1.5i)\\ +\ \text{Sin}(1.5j + 2.2j) + \text{Sin}(1.1i - 1.1j)\end{pmatrix} \tag{11}$$

Here (i, j) represents the spatial position. The artificially corrupted test images for performing quantitative and qualitative analysis of different algorithms are formed by adding $N_1 + N_2$ noise to uncorrupted synthetic images. The value of strength parameter, a is set in the interval [0.1 0.9] to corrupt the images.

The corrupted images are symmetrically padded with 30 rows and columns for avoiding the border effects in the restored images. For performing quantitative subjective/objective analysis of filtering algorithms, the metrics such as mean absolute error (MAE), peak signal-to-noise ratio (PSNR), mean structural similarity index measure (MSSIM) [39] and computation time (CT) in seconds are used. Formulations of MAE, PSNR and MSSIM are as in [7, 29–38]. An effective algorithm needs to produce high-quality restored outputs with higher PSNR and MSSIM values and lower MAE and CT values.

Since textural features in natural images have similar visual appearances like quasi-periodic noises, it is important to analyse the effectiveness of comparative filters in differentiating textural features from noisy counterparts and thereby maintaining textural features in its restored outputs. Tables 1–5 show the quantitative results of various algorithms in terms of MAE, PSNR, MSSIM and CT while restoring Lena, Boats, Bridge, Barbara and Parrot images contaminated by $N_1 + N_2$ type noise with a values equal to 0.1, 0.5 and 0.9.

Quantitative results in Tables 1–3 provide the insight of the performance of various algorithms in restoring lesser textured images with different levels of edge details. From the objective metrics, it is seen that Federic *et al.* filter provides closer results with proposed algorithm when restoring images contaminated with lower quantum of noises while WASMF is closer to the proposed algorithm when restoring images contaminated with higher quantum of noises. Quantitative results on Barbara and Parrot images shown in Tables 4 and 5 are used for analysing the performance of different algorithms in restoring textured images. From Tables 4 and 5, it is visible that although WASMF is closer in terms of quantitative metrics with the proposed algorithm at all

noise levels, the proposed algorithm is better in restoring images with textural details.

Further, it is clearly visible that the AGNF produces better PSNR and MSSIM values than the next best LFDF,WASMF, BRF and GNRF algorithms. Table 6 shows the average results of various algorithms while restoring ten standard images contaminated with $N_1 + N_2$ noise. From Table 6, it is found that the average values of all quantitative metrics are better for the proposed AGNF; MAE for AGNF being least followed by GNRF with a slightly higher value, PSNR being the highest for AGNF followed by LFDF,

Table 1 Quantitative comparison of algorithms for restored Lena images from $N_1 + N_2$ noise with different noise strength a

De-noising methods	Noise strength $a = 0.1$				Noise strength $a = 0.5$				Noise strength $a = 0.9$			
	MAE	PSNR	MSSIM	CT	MAE	PSNR	MSSIM	CT	MAE	PSNR	MSSIM	CT
ILPF	4.31	31.29	0.96	**0.33**	7.50	23.96	0.90	**0.34**	11.10	19.33	0.84	**0.34**
FDMF1	11.84	23.14	0.75	10.67	58.44	9.35	0.29	10.20	104.78	4.27	0.16	10.13
FDMF2	9.27	25.44	0.79	13.56	42.41	12.24	0.34	13.18	77.44	7.12	0.18	13.97
WGNF	4.17	29.17	0.95	13.32	17.45	16.93	0.71	13.38	31.00	12.04	0.55	13.52
GSF	3.01	30.15	0.98	2.92	9.19	18.36	0.91	9.60	13.78	14.24	0.88	15.99
Chakraborthy *et al.* filter	3.44	33.77	0.94	3.49	30.13	15.56	0.44	6.13	54.62	10.41	0.28	8.59
AONF	3.77	34.10	0.68	2.36	19.12	19.92	0.25	2.27	33.97	14.95	0.14	2.33
IF	10.00	25.93	0.88	6.35	19.14	19.76	0.65	6.30	27.38	16.03	0.51	6.42
BRF	2.28	37.27	0.98	4.34	10.05	23.81	0.81	4.21	18.94	18.13	0.66	4.19
GNRF	1.69	37.43	0.99	5.16	6.97	24.06	0.92	5.15	13.12	18.25	0.83	5.10
Federic *et al.* filter	1.61	40.19	0.99	3.59	**3.75**	30.75	0.93	3.37	**5.43**	27.01	0.86	4.23
WASMF	2.61	37.40	0.97	2.09	4.35	32.09	0.93	2.79	6.98	27.67	0.86	3.04
LFDF	1.97	39.26	0.98	2.27	5.16	30.71	0.91	2.75	8.12	26.74	0.83	3.19
AGNF	**1.28**	**43.29**	**1.00**	1.73	4.22	**32.66**	**0.95**	1.77	7.39	**27.71**	**0.88**	1.87

Bold values indicates the best experimental values obtained for all criteria among different algorithms.

Table 2 Quantitative comparison of algorithms for restored Boats images from $N_1 + N_2$ noise with different noise strength a

De-noising methods	Noise strength $a = 0.1$				Noise strength $a = 0.5$				Noise strength $a = 0.9$			
	MAE	PSNR	MSSIM	CT	MAE	PSNR	MSSIM	CT	MAE	PSNR	MSSIM	CT
ILPF	6.39	28.33	0.94	**0.31**	9.25	23.24	0.90	**0.34**	12.62	19.07	0.84	**0.31**
FDMF1	12.12	22.99	0.78	10.50	58.86	9.29	0.33	10.93	105.74	4.21	0.19	10.73
FDMF2	9.23	25.42	0.83	13.49	43.25	12.16	0.38	14.18	77.53	7.12	0.22	13.98
WGNF	4.54	29.07	0.96	13.18	17.82	16.78	0.74	13.30	31.48	11.92	0.58	14.24
GSF	3.47	29.68	0.98	2.66	9.86	18.15	0.92	8.28	14.92	13.83	0.89	13.31
Chakraborthy *et al.* filter	3.54	33.66	0.95	3.52	28.90	15.95	0.50	5.82	54.49	10.39	0.32	7.66
AONF	4.13	33.19	0.78	2.26	20.81	19.06	0.32	2.22	32.95	15.11	0.21	2.24
IF	9.06	25.70	0.91	6.29	16.63	20.84	0.72	6.29	26.33	16.38	0.55	6.35
BRF	2.60	36.55	0.98	4.47	10.17	23.77	0.84	4.33	18.92	18.18	0.70	4.35
GNRF	2.04	36.88	0.99	5.22	7.12	24.03	0.93	5.19	14.36	18.14	0.82	5.17
Federic *et al.* filter	2.37	37.22	0.99	3.28	4.55	29.65	0.95	3.61	**6.26**	26.01	0.88	5.05
WASMF	3.27	35.07	0.96	2.10	**4.35**	32.16	0.95	2.76	7.22	27.40	0.88	3.02
LFDF	2.11	38.85	0.98	2.64	5.14	30.77	0.93	2.70	8.10	26.83	0.86	3.15
AGNF	**1.85**	**40.34**	**0.99**	1.68	4.52	**32.26**	**0.96**	1.81	7.58	**27.58**	**0.90**	1.86

Bold values indicates the best experimental values obtained for all criteria among different algorithms.

Table 3 Quantitative comparison of algorithms for restored Bridge images from $N_1 + N_2$ noise with different noise strength a

De-noising methods	Noise strength $a = 0.1$				Noise strength $a = 0.5$				Noise strength $a = 0.9$			
	MAE	PSNR	MSSIM	CT	MAE	PSNR	MSSIM	CT	MAE	PSNR	MSSIM	CT
ILPF	10.13	24.95	0.92	**0.33**	12.37	21.89	0.90	**0.35**	15.35	18.50	0.86	**0.35**
FDMF1	12.44	22.68	0.87	10.82	59.31	9.22	0.41	11.52	10.97	4.19	0.24	11.60
FDMF2	10.98	24.19	0.89	11.51	43.11	12.08	0.48	13.40	76.65	7.14	0.28	13.24
WGNF	5.52	27.78	0.98	11.88	19.32	16.14	0.82	13.01	33.41	11.53	0.67	14.07
GSF	4.08	29.50	0.99	3.04	10.48	18.30	0.95	10.28	15.10	14.28	0.92	17.10
Chakraborthy *et al.* filter	3.57	33.60	0.98	3.45	16.97	19.85	0.78	3.28	52.63	10.81	0.41	8.45
AONF	3.83	34.10	0.92	2.36	18.64	20.19	0.51	2.23	33.50	15.10	0.31	2.35
IF	15.72	21.62	0.87	6.42	21.45	18.93	0.75	6.36	29.97	15.60	0.62	6.49
BRF	2.97	35.68	0.99	4.45	10.26	23.75	0.91	4.34	18.95	18.27	0.81	4.33
GNRF	**2.41**	36.23	**1.00**	5.18	9.37	23.32	0.94	5.15	15.51	17.98	0.87	5.09
Federic *et al.* filter	6.55	28.22	0.93	3.98	8.28	26.07	0.92	3.98	9.78	24.09	0.91	5.27
WASMF	4.08	32.19	0.96	2.10	5.26	30.92	0.97	2.73	**7.79**	27.04	0.94	2.96
LFDF	3.01	36.00	0.99	2.26	5.43	30.41	0.97	2.74	8.39	26.61	0.93	3.11
AGNF	2.53	**37.67**	0.99	1.59	**4.90**	**31.57**	**0.98**	1.80	7.84	**27.30**	**0.95**	1.84

Bold values indicates the best experimental values obtained for all criteria among different algorithms.

Table 4 Quantitative comparison of algorithms for restored Barbara images from $N_1 + N_2$ noise with different noise strength a

De-noising methods	Noise strength $a = 0.1$				Noise strength $a = 0.5$				Noise strength $a = 0.9$			
	MAE	PSNR	MSSIM	CT	MAE	PSNR	MSSIM	CT	MAE	PSNR	MSSIM	CT
ILPF	9.01	24.41	0.87	**0.32**	11.86	21.61	0.82	**0.35**	15.22	18.37	0.77	**0.34**
FDMF1	12.05	23.01	0.79	10.37	58.66	9.31	0.32	10.88	105.19	4.23	0.17	11.73
FDMF2	9.39	25.37	0.84	13.50	43.31	12.11	0.37	13.20	77.50	7.12	0.20	12.97
WGNF	4.65	28.87	0.96	13.26	18.68	16.36	0.74	13.33	31.64	11.86	0.59	13.34
GSF	3.37	29.87	0.98	3.12	9.55	18.49	0.93	10.58	13.84	14.58	0.89	18.80
Chakraborthy *et al.* filter	3.53	33.70	0.95	3.64	28.30	16.08	0.52	6.09	53.73	10.54	0.31	6.73
AONF	3.78	34.12	0.76	2.30	20.35	19.30	0.35	2.33	36.62	14.20	0.22	2.33
IF	10.15	25.32	0.87	6.36	16.45	20.93	0.73	6.43	26.10	16.37	0.57	6.49
BRF	2.67	36.26	0.98	4.41	10.26	23.77	0.85	4.32	18.77	18.30	0.73	4.30
GNRF	3.92	32.73	0.96	4.48	7.87	23.83	0.91	4.44	14.04	18.19	0.84	4.42
Federic *et al.* filter	8.38	24.97	0.88	3.91	8.48	24.91	0.90	3.73	9.48	24.20	0.88	5.12
WASMF	2.81	36.79	0.97	1.93	4.80	31.51	0.94	2.80	**7.32**	27.46	0.89	3.07
LFDF	3.86	33.32	0.97	2.74	5.34	30.57	0.93	2.69	8.39	26.57	0.86	3.15
AGNF	**1.70**	**40.16**	**0.99**	1.67	**4.55**	**32.03**	**0.96**	1.83	7.65	**27.49**	**0.91**	1.97

Bold values indicates the best experimental values obtained for all criteria among different algorithms.

Table 5 Quantitative comparison of algorithms for restored Parrot images from $N_1 + N_2$ noise with different noise strength a

De-noising methods	Noise strength $a = 0.1$				Noise strength $a = 0.5$				Noise strength $a = 0.9$			
	MAE	PSNR	MSSIM	CT	MAE	PSNR	MSSIM	CT	MAE	PSNR	MSSIM	CT
ILPF	11.20	22.81	0.75	**1.50**	15.24	22.98	0.74	**0.72**	12.36	22.43	0.69	**0.53**
FDMF1	9.79	24.73	0.70	15.55	17.97	11.21	0.22	20.75	86.02	6.13	0.11	20.61
FDMF2	6.61	27.78	0.81	20.82	30.01	14.99	0.33	19.97	53.10	10.03	0.19	20.49
WGNF	3.64	30.34	0.94	21.96	12.62	19.54	0.72	20.82	21.88	14.66	0.56	21.05
GSF	2.36	31.57	0.98	4.86	7.69	19.55	0.90	13.74	11.37	15.65	0.86	22.92
Chakraborthy *et al.* filter	3.68	32.86	0.90	6.10	22.15	17.25	0.46	4.97	46.00	11.08	0.26	11.64
AONF	4.50	32.01	0.48	3.79	22.74	17.96	0.13	3.48	40.92	12.85	0.07	3.42
IF	8.32	26.10	0.86	10.60	17.78	20.18	0.62	9.65	25.53	16.70	0.45	9.78
BRF	2.32	36.48	0.97	7.14	10.09	23.84	0.73	6.38	17.56	18.72	0.58	6.47
GNRF	2.61	35.36	0.97	8.54	7.48	23.66	0.86	7.71	12.93	18.41	0.75	7.70
Federic *et al.* filter	1.92	36.25	0.98	5.29	4.85	31.27	0.90	4.37	7.64	28.93	**0.88**	4.72
WASMF	2.31	35.25	0.97	4.96	4.83	30.56	0.89	4.37	7.87	26.30	0.78	4.53
LFDF	1.89	36.48	0.98	11.15	3.98	31.45	0.91	11.04	6.51	28.98	0.84	11.29
AGNF	**1.38**	**41.03**	**0.99**	2.17	**3.42**	**32.10**	**0.92**	2.54	**7.48**	**29.34**	**0.88**	2.14

Bold values indicates the best experimental values obtained for all criteria among different algorithms.

Table 6 Average quantitative results of 25 restored images from $N_1 + N_2$ noise of different noise strength a

De-noising methods	Noise strength $a = 0.1$				Noise strength $a = 0.5$				Noise strength $a = 0.9$			
	MAE	PSNR	MSSIM	CT	MAE	PSNR	MSSIM	CT	MAE	PSNR	MSSIM	CT
ILPF	9.15	24.27	0.88	**0.45**	11.64	19.8	0.8	**0.19**	14.79	18.43	0.81	**0.34**
FDMF1	12.16	20.65	0.75	10.6	58.64	11.08	0.37	11.34	97.32	5.21	0.21	12.03
FDMF2	9.27	27.13	0.77	13.69	43.11	13.1	0.42	13.63	76.94	5.12	0.17	13.14
WGNF	5.12	30.34	0.93	13.39	18.96	17.76	0.69	13.63	32.02	12.6	0.58	13.84
GSF	3.67	29.75	0.91	3.4	10.08	16.38	0.95	10.3	14.62	12.58	0.84	17.57
Chakraborthy *et al.* filter	3.43	31.86	0.92	3.59	25.63	14.54	0.58	5.59	53.74	9.78	0.32	7.27
AONF	3.41	33.5	0.81	2.61	19.78	19.71	0.38	2.15	35.42	13.7	0.22	2.43
IF	9.74	26.05	0.84	6.51	16.58	22.12	0.73	6.39	26.04	17.51	0.54	6.81
BRF	2.97	36.56	0.95	4.42	10.09	24.49	0.8	4.13	19.02	15.62	0.75	4.29
GNRF	3.09	33.57	0.97	5.11	7.95	22.01	0.96	4.71	13.95	17.78	0.77	4.97
Federic *et al.* filter	6.66	27.73	0.95	3.81	7.68	25.29	0.93	4.03	8.51	23.86	0.9	5.46
WASMF	2.95	33.75	0.96	1.97	4.67	29.38	**0.97**	3.02	**7.37**	26.72	0.92	3.22
LFDF	3.65	32.5	0.94	2.8	5.33	29.2	0.96	3.14	8.59	27.92	0.82	3.49
AGNF	**2.04**	**39.61**	**0.98**	1.8	**4.22**	**30.88**	**0.97**	1.82	7.39	**29.02**	**0.93**	2.21

Bold values indicates the best experimental values obtained for all criteria among different algorithms.

MSSIM being highest for AGNF and GRNF. Though all algorithms have $O(n^2)$ complexity in frequency domain, the time taken to run the proposed AGNF is the least when compared to most other adaptive filters in the comparative study under the same experimental conditions. Thus, Tables 1–6 demarcates the effectiveness of the proposed AGNF algorithm in providing better objective and subjective metric values than other comparative algorithms.

Fig. 4 shows the restoration results produced by the proposed AGNF (Fig. 4*f*) and various frequency/spatial domain based

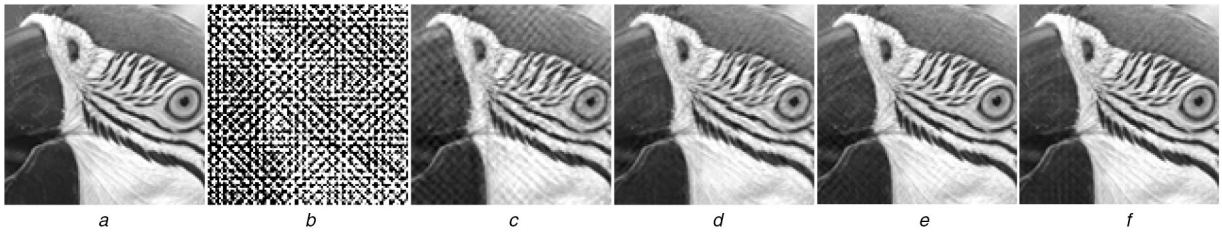

Fig. 4 *Restored Parrot images from $N_1 + N_2$ noise of strength $a = 0.5$*

(a) Original image, ***(b)*** Noisy image (PSNR: 6.80, MSSIM: 0.005), ***(c)*** WGNF (PSNR: 19.54, MSSIM: 0.72), ***(d)*** Federic *et al.* filter (PSNR: 31.27, MSSIM: 0.90), ***(e)*** LFDF (PSNR: 31.45, MSSIM: 0.91), ***(f)*** Proposed AGNF (PSNR: 32.10, MSSIM: 0.92)

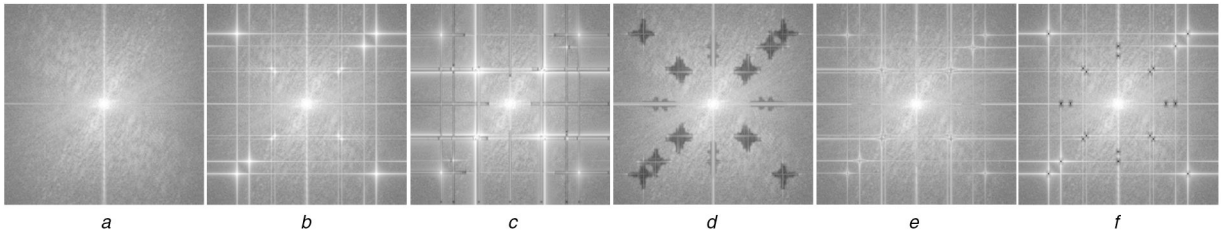

Fig. 5 *Fourier transform of restored Parrot images from $N_1 + N_2$ noise of strength $a = 0.5$*

(a) Fourier transform of Fig. 4*a*, ***(b)*** Fourier transform of Fig. 4*b*, ***(c)*** Fourier transform of Fig. 4*c*, ***(d)*** Fourier transform of Fig. 4*d*, ***(e)*** Fourier transform of Fig. 4*e*, ***(f)*** Fourier transform of Fig. 4*f*

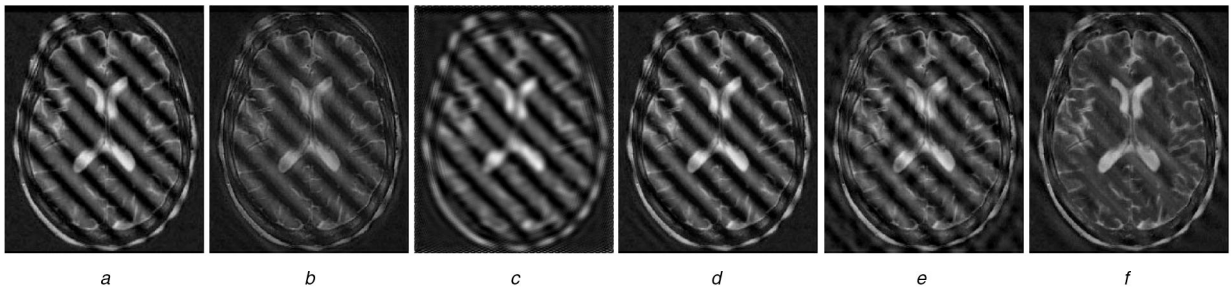

Fig. 6 *Restored results of different algorithms from naturally corrupted brain MRI images*

(a) Input image, ***(b)*** WGNF, ***(c)*** GNRF, ***(d)*** Federic *et al.* filter, ***(e)*** LFDF, ***(f)*** Proposed AGNF

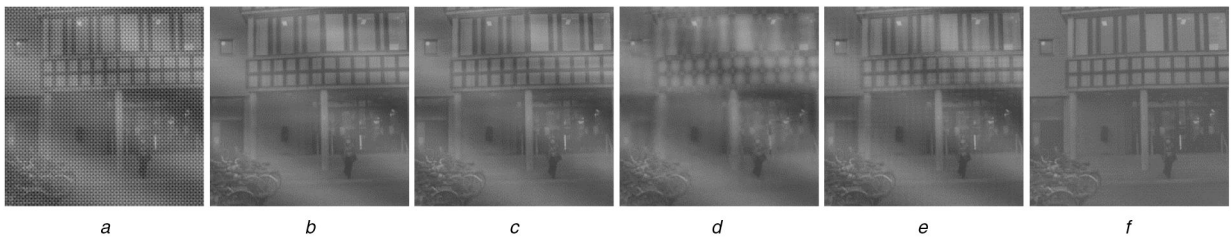

Fig. 7 *Restored results of different algorithms from naturally corrupted street images*

(a) Input image, ***(b)*** WGNF, ***(c)*** GNRF, ***(d)*** Federic *et al.* filter, ***(e)*** LFDF, ***(f)*** Proposed AGNF

comparative algorithms (Figs. 4*c–e*) from cropped version of noisy Parrot image contaminated by $N_1 + N_2$ noise with $a = 0.5$.

Fig. 5 shows the Fourier transform of restored Parrot images by different frequency domain based algorithms corresponding to Fig. 4. From Figs. 4 and 5, it is seen that Federic *et al.* filter and LFDF perform well in restoring noisy peaks created in Fig. 5*b* by the noisy sinusoidal functions corresponding to periodic noises in Fig. 4*b*. The results produced by Federic *et al.* filter though are arbitrarily close to the results of AGNF, the proposed AGNF produces slightly better results as can be understood from the Fourier transform of Figs. 4*c–f* in Figs. 5*c–f*.

The misclassifications of noisy peak areas by the comparative filters in the restoration phase are also vivid in Figs. 5*c–e*. Figs. 6 and 7 show the restored results of top ranking algorithms from naturally corrupted Brain MRI and Street images, respectively. The images restored by the proposed AGNF (Figs. 6*f* and 7*f*) though have some visual similarity with LFDF (Figs. 6*e* and 7*e*), AGNF shows good improvements in visual quality while comparing the restored images produced by WGNF (Figs. 6*b* and 7*b*), GNRF (Figs. 6*c* and 7*c*) and Federic *et al.* filters (Figs. 6*d* and 7*d*). Fig. 8 shows the naturally corrupted images of different applications. Restored images produced by AGNF (Figs. 9*a–f*) from naturally corrupted images in Figs. 8*a–f* demarcate the improved performance of the proposed AGNF while removing periodic noise from digital images.

In order to visually analyse the performance of algorithms in preserving edges, edge deviations in restored outputs by different algorithms using Canny edge detection [4] method are shown in Fig. 10. The red pixels are the edge pixels of the noise-free image that are not in the edge image of the restored image while blue pixels denote the wrongly introduced edges in the restored image that are not in the edge image of the noise-free image. The green pixels are the correctly retained edges of the restored outputs. From Fig. 10, it is clear that the edge retention errors in terms of red and blue pixels are less significant in numbers for the proposed algorithm (Fig. 10*f*) and it visually demarcates the improved capability of the proposed algorithm in preserving edges in its restored outputs than other algorithms (Figs. 10*b–e*).

Fig. 8 *Naturally corrupted images of different applications*
(a) Mariner 4 image, ***(b)*** Lower body MRI image, ***(c)*** Boy image, ***(d)*** Hand written image, ***(e)*** Live football match image, ***(f)*** Clown image

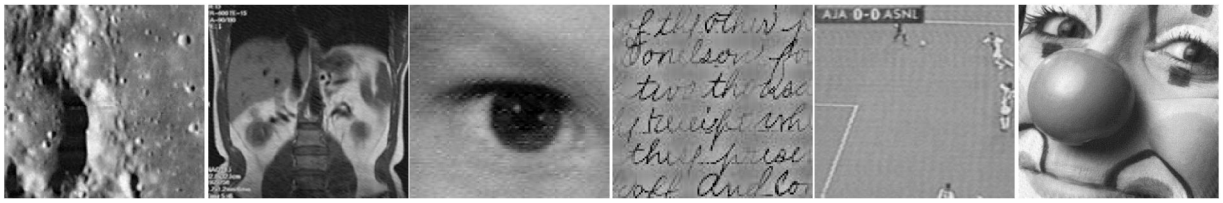

Fig. 9 *Restored images produced by AGNF from naturally corrupted images of different applications*
(a) De-noised Mariner 4 image, ***(b)*** De-noised Lower body MRI image, ***(c)*** De-noised Boy image, ***(d)*** De-noised Hand written image, ***(e)*** De-noised Live football match image, ***(f)*** De-noised Clown image

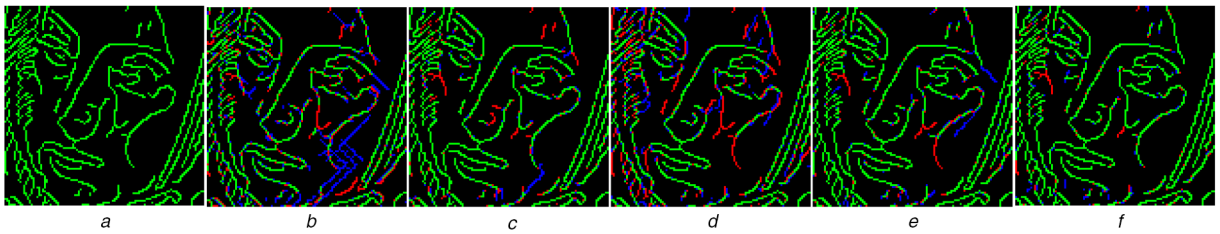

Fig. 10 *Edge deviations in restored images of corrupted Barbara image with $N_1 + N_2$ noise and $a = 0.05$ by different algorithms indicated as correctly retained (Green), not retained (Red) and wrongly introduced (Blue) edges*
(a) Original image, ***(b)*** AONF, ***(c)*** WGNF, ***(d)*** Federic *et al.* filter, ***(e)*** LFDF, ***(f)*** Proposed AGNF

4 Discussion and parameter analysis

The ILPF provides its best results when it allows only specific disc shaped LFR around DC coefficient with a maximum radius so that it does not meet nearest noisy peak of the corrupted frequency domain image and this rejection areas centred at DC coefficient are identified by trial and error approach. The FDMF1, FDMF2 and WGNF though perform well in detecting noisy peaks, they find difficulty in providing good restored results since they are not adaptive in fixing the window size. AONF requires quantification of circular LFR around DC coefficient for identifying global threshold to avoid these areas from noisy peak detection process.

However, the proposed algorithm does not require any such additional calculations since it works on local ratio based thresholding to identify noisy regions. This advantage of the proposed algorithm makes it skip the numerous calculations involved in finding LFR and the possible errors in fixing the radius of LFR areas. Since the noisy peak heights are locally varying by the strength of noise amplitude and are scattered in the frequency domain image in accordance with the noisy sinusoidal frequencies, the global threshold identified by AONF may not correctly identify smaller noisy peaks thereby leaving much of these noises unaltered in its restored images. Further, even in the absence of noise in images, this global threshold used by AONF may misclassify natural image frequency variations as noisy peaks.

Although the computational complexity of the algorithm in frequency domain is same as other algorithms in the comparison study, the proposed algorithm is faster than most other methods in terms of time taken in seconds (Tables 1–6). This is due to the fact that the proposed scheme does not need to employ additional calculations such as finding LFRs, global threshold and so on. The improved quantitative values obtained by AGNF tabulated in Tables 1–6 and the visual analysis on Figs. 4–7 clearly reveal the improved performance of the proposed algorithm particularly its accuracy in identifying noisy peak areas, efficacy in rejecting corrupted frequencies and capability in maintaining thin and narrow edges in the restored images.

The noise detection and correction window sizes of FDMF1, FDMF2 and WGNF are set to 7×7 as suggested by the authors. For WGNF and AONF, the parameters A and B of Gaussian notch filter are, respectively, set to 1.0 and 0.01 as the proposed AGNF algorithm. The GSF uses region-growing technique based on similarity of frequency values to quantify the noisy regions. So, the algorithm could not provide effective results due to unfeasible similarity checks employed in the exponentially decreasing noisy peak areas. Similar to the proposed algorithm, AONF performs noise quantification process by using adaptively varying inner and outer windows starting from sizes 3×3 and 5×5. AONF counts the number of frequency components of larger window that has a lower value than its corresponding comparison pixel in the lower window. If this count is more than half of the total outer pixels, the algorithm increases the size of both windows. The process continues until the condition fails. The region covered by last outer window is considered as the quantified area of noise contamination. However, this region growing criteria may lead to misclassifications in quantifying the noisy regions. Since the proposed algorithm uses threshold to check the ratio of relative deviation in frequency averages of outer frequencies with inner frequencies to decide the purity of inner frequencies, the proposed algorithm always provides better accuracy in quantifying noisy peak regions than AONF and GSF.

Although the noisy peak detection procedures employed by IF, BRF and GNRF are effective, these algorithms do not quantify the noisy areas around it. The filtering window width for IF, BRF and GNRF are, respectively, set to 9, 8 and 9 in brick wall and cross shapes as suggested by the authors. WASMF, LFDF Federic *et al.* filters use static thresholding functions for detecting noisy frequencies and these functions are not adaptive to varying strength and type of corrupting noises. Other parameters associated with

Table 7 PSNR achieved with different threshold values while de-noising images contaminated with $N_1 + N_2$ noise

Images	Noise strength, *a*	Values of threshold, *T*							
		T = 0.2	*T* = 0.25	*T* = 0.3	*T* = 0.35	*T* = 0.4	*T* = 0.45	*T* = 0.5	*T* = 0.55
Barbara	0.1	19.96	40.41	**40.67**	40.16	40.10	39.29	29.10	25.58
	0.5	6.01	31.13	31.91	**32.03**	31.79	31.95	27.43	24.73
	0.9	0.91	27.26	27.40	27.49	**27.52**	27.12	25.77	23.63
Lena	0.1	19.98	40.98	43.27	**43.29**	43.28	42.15	37.91	35.35
	0.5	6.01	31.58	32.53	**32.66**	32.40	33.74	33.05	32.31
	0.9	0.91	27.47	27.67	27.71	**27.82**	26.82	26.61	26.28
Boats	0.1	19.96	40.47	**40.50**	40.34	39.97	36.12	33.35	30.21
	0.5	6.01	31.38	32.14	**32.26**	31.66	31.51	30.36	28.11
	0.9	0.91	27.14	27.45	27.58	27.19	27.01	26.87	26.67
Bridge	0.1	19.93	37.41	**37.84**	37.67	37.45	36.44	25.85	23.95
	0.5	6.01	31.11	31.47	**31.57**	31.13	30.38	24.59	23.89
	0.9	0.91	26.83	27.54	27.30	**27.36**	26.79	23.44	22.89
Baboon	0.1	19.92	36.53	**36.76**	36.22	35.58	32.98	30.67	26.28
	0.5	6.01	30.44	30.79	**30.87**	30.61	28.71	27.60	24.89
	0.9	0.91	26.72	26.87	**26.99**	26.73	26.49	25.03	23.77

Bold values indicates the best experimental values obtained for all criteria among different algorithms.

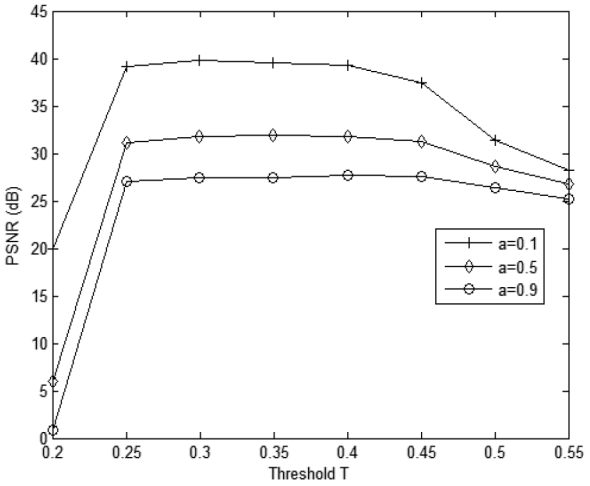

Fig. 11 *Plot of average PSNR values recorded while de-noising images affected with $N_1 + N_2$ noise of different strengths*

FDMF1, FDMF2, WGNF, GSF, Chakraborty *et al.*, AONF, IF, BRF, GNRF, Federic *et al.*, WASMF and LFDF algorithms are set as suggested by the authors.

In contrast to these algorithms, the proposed AGNF algorithm need only to optimise the threshold, T used for peak and noisy region identification. The optimum value of T largely depends on the height and width of the noisy peak area that in turn depends on the noise amplitude of corrupting noise. Optimisation of T requires either a rough estimation of corrupting noise/noisy peak areas or a trained neural/genetic/deep learning algorithm and these processes require additional calculations. To speed up the process by avoiding these additional calculations, this study attempted a reasonable estimation of T by performing empirical analysis. Numerous experiments are conducted by varying the value of T, noise types, noise strength and images to arrive at a reasonable value for T from which the images added with $N_1 + N_2$ noise are discussed in this paper. The average PSNR values of AGNF algorithm for varying T from different images corrupted with $N_1 + N_2$ noise are provided in Table 7. The plot of average PSNR values from 25 restored images with different noise strength between threshold values is shown in Fig. 8. Fig. 11 shows that the performance of AGNF is reasonably stable when T is in the range [0.25 0.4]. Based on these results, the value of T is set as $T = 0.35$ for all experiments although better optimisation can be attempted by performing rough estimation of noise or by applying trained neural network/deep learning/genetic algorithms as a future work.

5 Conclusion

The paper presented an AGNF in Fourier transform domain for effectively restoring images contaminated with periodic, quasi-periodic and Moiré pattern noises. The frequency domain based proposed algorithm has the capability of adaptively detecting and quantifying noisy peak areas for diffusing these noisy peaks by Gaussian notch filter of adaptively varying sizes. Experimental analysis conducted under different test conditions on various images proved that the ratio based region-growing criteria of the proposed algorithm provides better accuracy in detecting and quantifying noisy peak regions in frequency domain images. Qualitative and quantitative result analysis demarcated that AGNF produces better restored outputs and is capable of retaining edges and textural features in its restored outputs than other comparative methods used in the experimental study.

6 References

[1] Kursat, G.B., Li, X.: '*Image restoration: fundamentals and advances*' (CRC Press, New York, USA., 2012).

[2] Milan, S., Hlavac, V., Boyle, R.: '*Image processing analysis, and machine vision*' (Cengage Learning, Boston, 2014, 4th edn.)

[3] Saudia, S., Varghese, J., Nallaperumal, K., *et al.*: 'Salt & pepper impulse detection and median based regularization using adaptive median filter'. Proc. Int. Conf. IEEE Region 10 TENCON, November 2008, pp. 1–6

[4] Gonzalez, R.C., Woods, R.E.: '*Digital image processing*' (Pearson Prentice Hall, New Jersey, USA., 2008, 3rd edn.)

[5] Chen, Y.Y., Kashti, T., Fischer, M., *et al.*: 'The lattice-based screen set: A square-color all-orders Moiré-free screen set', *IEEE Trans. Image Process.*, 2016, **25**, (4), pp. 1873–1886

[6] Yunfei, L.: 'Observation of electron beam Moiré fringes in an image conversion tube', *Ultramicroscopy*, 2016, **170**, pp. 19–23

[7] Moallem, P., Masoumzadeh, M., Habibi, M.: 'A novel adaptive Gaussian restoration filter for reducing periodic noises in digital image', *Signal. Image. Video. Process.*, 2013, **9**, (5), pp. 1179–1191

[8] Frédéric, S., Grediac, M.: 'Sensor noise modeling by stacking pseudo-periodic grid images affected by vibrations', *IEEE Signal Process. Lett.*, 2014, **21**, (4), pp. 432–436

[9] Yuanhe, T.: 'Beyond the partial light intensity imager: eliminating Moiré patterns', *Opt. Commun.*, 2015, **355**, (11), pp. 143–147

[10] Hamed, A.M., Al-Saeed, T.A.: 'Reconstruction of the corneal layers affected by a periodic noise application on microscopic interferometry', *Int. J. Phot. Opt. Tech 2*, 2016, **3**, pp. 6–12

[11] Zhouping, W.: 'A median-Gaussian filtering framework for Moiré pattern noise removal from X-ray microscopy image', *Micron*, 2012, **43**, (2), pp. 170–176.

[12] Katarzyna, K., Bekiesińska-Figatowska, M.: 'Artifacts in magnetic resonance imaging', *Polish J. Radiol.*, 2015, **80**, (2), pp. 93–106

[13] Bruno, C., Dooms, A., Cornelis, J., *et al.*: 'Digital canvas removal in paintings', *Signal Process.*, 2012, **92**, (4), pp. 1166–1171

[14] Sabine, H.: 'From A as in aliasing to Z as in zipper: artifacts in MRI', *Clin. Neuroradiol.*, 2008, **18**, (1), pp. 25–36

[15] Yi-Hsuan, K., MacFall, J.R.: 'Correction of MR k-space data corrupted by spike noise', *IEEE Trans. Med. Imaging*, 2006, **19**, (7), pp. 671-680.

[16] Ding, W., Li, A., Wu, J., *et al.*: 'Automatic macroscopic density artefact removal in a nissl-stained microscopic atlas of whole mouse brain', *J. Microsc.*, 2013, **251**, (2), pp. 168–177.

[17] Michel, G., Frédéric, S., Blaysat, B.: 'Removing quasi-periodic noise in strain maps by filtering in the Fourier domain', *Exp. Tech.*, 2016, **40**, (3), pp. 959–971
[18] Chang, Y., Yan, L., Fang, H., *et al.*: 'Anisotropic spectral-spatial total variation model for multispectral remote sensing image destriping', *IEEE Trans. Image Process.*, 2015, **24**, (6), pp. 1852–1866
[19] Dou, H.X., Huang, T.Z., Deng, L.J., *et al.*: 'Directional ℓ0 sparse modeling for image stripe noise removal', *Remote Sens.*, 2018, **10**, (3), p. 361.
[20] Xiao, P., Yecai, G., Peixian, Z.: 'Removing stripe noise from infrared cloud images via deep convolutional networks.', *IEEE Photonics J.*, 2018, **10**, (4), pp. 1–14.
[21] Atul, R.: '*An empirical study of periodic noise filtering in Fourier domain: an introduction to novel autonomous periodic noise removal algorithms*' (LapLambert Academic Publishing, Saarland, 2013)
[22] Aizenberg, I., Butakoff, C.: 'Nonlinear frequency domain filter for quasi periodic noise removal'. Proc. Int. Workshop on Spectra Methods and Multirate Signal Processing, Toulouse, France, 2002
[23] Aizenberg, I., Butakoff, C.: 'Frequency domain median like filter for periodic and quasi-periodic noise removal'. Proc. Int. Conf. on Image Processing: Algorithms and Systems, San Jose, CA, USA., May 2002, pp. 181-191.
[24] Aizenberg, I., Butakoff, C.: 'A windowed Gaussian notch filter for quasi-periodic noise removal', *Image Vis. Comput.*, 2008, **26**, (10), pp. 1347–1353
[25] Anastasios, K.C., Olivo, A., Munro, P.R.T., *et al.*: 'Optical characterisation of a CMOS active pixel sensor using periodic noise reduction techniques', *Nucl. Instrum. Methods Phys. Res., Sect. A*, 2010, **620**, (2), pp. 549–556.
[26] Ketenci, S., Gangal, A.: 'Design of Gaussian star filter for reduction of periodic noise and quasi-periodic noise in gray level images'. Proc. Int. Conf. on Innovations in Intelligent Systems and Applications, Trabzon, Turkey, 2012, pp. 1–5.
[27] Hudhud, G.A., Turner, M.J.: 'Digital removal of power frequency artifacts using a Fourier space median filter', *IEEE Signal Process. Lett.*, 2005, **12**, (8), pp. 573–576.
[28] Chakraborty, D., Tarafder, M.K., Chakraborty, A., *et al.*: 'A proficient method for periodic and quasi-periodic noise fading using spectral histogram thresholding with sinc restoration filter', *AEU-Int. J. Electron. Commun.*, 2016, **70**, (12), pp. 1580–1592.
[29] Frédéric, S., Grédiac, M.: 'Automated removal of quasiperiodic noise using frequency domain statistics', *J. Electron Imaging*, 2015, **24**, (1), p. 13003
[30] Varghese, J., Subash, S., Tairan, N.: 'Fourier transform-based windowed adaptive switching minimum filter for reducing periodic noise from digital images', *IET Image Process.*, 2016, **10**, (9), pp. 646–656.
[31] Varghese, J., Subash, S., Tairan, N., *et al.*: 'Laplacian-based frequency domain filter for the restoration of digital images corrupted by periodic noise', *Can. J. Electr. Comput. Eng.*, 2016, **39**, (2), pp. 82–91
[32] Chakraborty, D., Chakraborty, A., Banerjee, A., *et al.*: 'Automated spectral domain approach of quasi-periodic denoising in natural images using notch filtration with exact noise profile', *IET Image Process.*, 2018, **12**, (7), pp. 1150–1163.
[33] Ketenci, S., Ali, G.: 'Automatic reduction of periodic noise in images using adaptive Gaussian star filter 2', *Turkish J. Electr. Eng. Comput. Sci.*, 2017, **25**, (9), pp. 2336–2348
[34] Ionita, M., Coanda, H.: 'Wavelet and Fourier decomposition based periodic noise removal in microscopy images', *Sci. Bulletin Electr. Eng. Faculty*, 2018, **38**, (1), pp. 68–71
[35] Zhou, W., Yunjie, Z., Yongchao, L.: 'Bilateral linear operator for period noise image De-noising'. Proc. ACM Int. Conf. Computer Science and Application Engineering, Hohhot, People's Republic of China, October 2018, pp. 1–5.
[36] Chakraborty, D., Milan, K.T., Ayan, B., *et al.*: 'Gabor-based spectral domain automated notch-reject filter for quasi-periodic noise reduction from digital images', *Multimedia Tools Appl.*, 2019, **78**, (2), pp. 1757–1783
[37] Varghese, J.: 'Frequency-domain-based switching median filter for the restoration of images corrupted with high-density periodic noise', *Scientia Iranica, Trans. D, Comput. Sci. Eng., Electr.*, 2017, **24**, (3), pp. 1312–1324
[38] Varghese, J.: 'Adaptive threshold based frequency domain filter for periodic noise reduction', *AEU-Int. J. Electron. Commun.*, 2016, **70**, (12), pp. 1692–1701.
[39] Wang, Z., Bovik, A.C., Sheikh, H.R., *et al.*: 'Image quality assessment: from error visibility to structural similarity', *IEEE Trans. Image Process.*, 2004, **13**, (4), pp. 600-612.